Research Article Vol. 33, No. 10 / 19 May 2025 / Optics Express 20399
Optics EXPRESS

SESAM mode-locked Nd:fiber laser at 920 nm for nonlinear optical microscopy

FEDELE PISANI,[1,2,*] GABRIELE DI NOIA,[3] FRANCESCO CRISAFI,[3] MATTEO NEGRO,[3] GIULIO CERULLO,[1,2,3] AND GIANLUCA GALZERANO[2]

[1]Dipartimento di Fisica - Politecnico di Milano, Piazza Leonardo da Vinci 32, 20133 Milano, Italy
[2]Istituto di Fotonica e Nanotecnologie - Consiglio Nazionale delle Ricerche, Piazza Leonardo da Vinci 32, 20133 Milano, Italy
[3]Cambridge Raman Imaging S.r.l., PoliHub, Via Durando 39, 20158 Milano, Italy
*fedele.pisani@polimi.it

Abstract: We report on the design, modeling, and characterization of a diode-pumped Nd-doped all-polarization-maintaining fiber laser operating at 920 nm in a passively mode-locked regime enabled by a SESAM. The laser generates pulse trains with a repetition frequency of 18.5 MHz and an average output power of 0.26 mW in an optical bandwidth of 0.6 nm. Within the broad integration bandwidth from 50 Hz to 9.25 MHz, the Nd:fiber laser exhibits ultra-low intensity noise, at a relative level of 0.04%, and timing jitter below 2 ps. Moreover, we demonstrate the ability to lock the laser's repetition frequency to that of an Yb-doped oscillator, enabling stimulated Raman scattering microscopy in the fingerprint region.

1. Introduction

Biomedical imaging techniques such as coherent Raman scattering microscopy rely heavily on ultrafast lasers capable of generating stable, ultrashort pulses in the near-infrared with exceptional spectral and temporal precision [1]. Stimulated Raman scattering (SRS) microscopy, in particular, requires two synchronized laser pulses of different colors, the pump and the Stokes, whose frequency difference matches a vibrational frequency of the sample, and measures the amplification of the Stokes pulse (stimulated Raman gain) or the attenuation of the pump pulse (stimulated Raman loss) mediated by coherent molecular vibrations [2,3].

Among coherent Raman imaging techniques, SRS offers several advantages, such as the linear dependence of the signal on the concentration of molecules and the absence of non-resonant background; it is therefore emerging as a powerful method for high-speed label-free chemical imaging of cells and tissues, with numerous biomedical applications in research and diagnostics [4,5]. So far, SRS microscopy has been mostly implemented in a single-frequency (narrowband) configuration, recording the signal at a specific pump-Stokes frequency detuning. Broadband SRS [6], on the other hand, measures a Raman spectrum for every pixel of the image, thus greatly increasing the amount of bio-chemical information extracted from the sample. It is, however, technically much more challenging, as it requires the combination of a narrowband pump beam with a broadband Stokes beam and the measurement of the SRS signal for every Stokes frequency.

A prerequisite for the translation of the SRS technique to real-world applications in biomedical research and diagnostics is the adoption of all-fiber-optic technologies, owing to their compactness, reliability and operational stability [7–12]. So far, all-fiber lasers for SRS microscopy have been developed in a narrowband configuration. Only recently, we demonstrated a novel all-fiber laser system for broadband SRS microscopy which combines two intrinsically, passively synchronized oscillators: a frequency-doubled Er:fiber laser providing a narrowband pump beam at 785 nm, and an Yb:fiber laser providing a broadband Stokes beam around 1040 nm [13,14]. This system allows us to cover the high frequency CH stretching region (2800 – 3100 cm^{-1}) of the vibrational

#557820 https://doi.org/10.1364/OE.557820
Journal © 2025 Received 24 Jan 2025; revised 26 Mar 2025; accepted 29 Mar 2025; published 6 May 2025

Optics EXPRESS

spectrum and record, using a high-frequency multi-channel lock-in amplifier [5], SRS spectra with pixel dwell times of a few microseconds.

While the CH stretching region already allows molecular identification, many applications call for the access to the highly chemically informative fingerprint region (1000 – 1700 cm^{-1}). This would be possible, in our configuration, by combining the broadband Yb:fiber Stokes laser and a narrowband pump laser with wavelength shifted to 920 nm. An effective approach to generate a train of ultrashort pulses at 920 nm is given by a mode-locked Nd-doped fiber laser operating on the quasi-three-level $^4F_{3/2}$-$^4I_{9/2}$ transition. Several studies have explored passive mode-locking of Nd at the 920 nm transition using artificial saturable absorbers, including the nonlinear amplifying loop mirror (NALM) method [15–18] and the nonlinear polarization evolution (NPE) method, both on its own [19,20] and in combination with a semiconductor saturable absorber mirror (SESAM) [21]. The use of a SESAM as the sole mode-locking element has been examined in both a ring cavity configuration [22] and, more recently, in a linear resonator design [23].

In this paper we report on the development and characterization of a 920 nm picosecond laser with an 18.5 MHz pulse repetition frequency, to be used as the pump beam for broadband SRS spectroscopy in the fingerprint region. Self-starting, passive mode-locking regime is obtained with a SESAM in a Nd-doped all-polarization-maintaining (PM) fiber linear oscillator design. Through a comprehensive approach involving both detailed simulations and experimental validations, we show that this laser meets the requirements as the pump source of a broadband SRS microscopy system in the fingerprint spectral region, generating few-picoseconds-long pulses at a central wavelength of 920 nm with a narrow 3 dB spectral bandwidth of 0.6 nm and average power of 0.26 mW. With Nd-doped fiber amplifiers, this power can be increased over 200 mW, meeting the demands of the SRS application. Moreover, this work presents, to our knowledge, the most comprehensive investigation of the stability of the intensity and pulse repetition frequency of a passively mode-locked Nd-doped fiber laser operating around 920 nm. Compared to previously reported results [15–23], this laser stands out for the low relative intensity noise (just 0.04% within an integration bandwidth from 50 Hz to 9.25 MHz), the excellent stability level of the pulse repetition frequency (better than 3.8×10^{-9} in fractional terms) and the low pulse timing jitter (below 2 ps). Lastly, we demonstrate the ability to passively lock the repetition frequency of the laser to that of an Yb-doped oscillator through cross-phase modulation (XPM) in a shared intracavity fiber [24], which will enable broadband SRS imaging in the vibrational fingerprint region.

2. Experimental setup

The experimental setup, illustrated in Fig. 1, features an all-fiber linear cavity with a 1-meter-long Nd-doped polarization-maintaining silica fiber (CorActive, Nd-103-PM) as the active medium. The output coupler consists of a fiber Bragg grating (FBG, Teraxion, custom design) with a 3 dB reflection bandwidth of 2 nm at 920 nm and a peak reflectivity of 88.3 %. Moreover, this device introduces on the reflected beam a group delay dispersion of $-2.97\ ps^2$, which determines the negative overall cavity dispersion, allowing solitonic mode-locking operation. Lastly, the FBG has very low reflectivity (R<0.1%) for the main transition line of Nd at 1064 nm, thus forcing laser operation on the lower gain 920 nm quasi-three-level transition. The active fiber is pumped by an FBG-stabilised diode laser at 808 nm with a maximum output power of 250 mW. An 808/920 wavelength division multiplexer (WDM, Ruik, HPMFWDM920/808) reflects the pump towards the active fiber through the FBG, which has high transmission (T = 95%) at 808 nm. The 920 nm output of the optical cavity is transmitted by the same WDM towards an optical isolator (Ruik, HPMIS-920).

Pulsed operation is achieved using a SESAM (Batop, SAM-920-30-3ps-15) designed for operation around 920 nm, with a 3 ps relaxation time, a 20 % modulation depth and a 10 % non-saturable absorption. A thermo-electric controller (developed in-house) keeps the device at

Optics EXPRESS

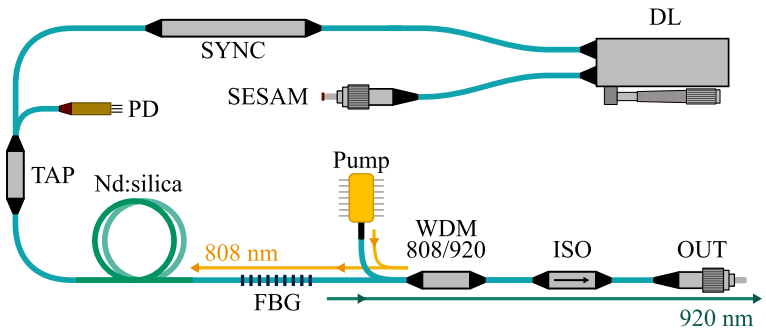

Fig. 1. Experimental layout of the passively mode-locked Nd:fiber laser. SYNC: synchronization system; DL: tunable optical delay line; SESAM: semiconductor saturable absorber mirror; PD: photodetector; TAP: 99/1% beam splitter; Pump: 808 nm pump diode; Nd:silica: Nd-doped active fiber; FBG: chirped fiber Bragg grating (output coupler); WDM 808/920: wavelength division multiplexer at 808/920 nm; ISO: optical isolator; OUT: FC/APC fiber connector at the output of the laser.

a constant temperature of 30 °C to avoid thermal fluctuations, thus improving the stability and reproducibility of the laser. A tunable optical delay line (DL, AFR, MDL-920-500-2-B-1-P) controls the pulse repetition frequency of the laser within ±100 kHz around 18.5 MHz with a resolution of 0.2 Hz, so that the unperturbed repetition frequency can be matched to that of a second unperturbed fiber oscillator. To suppress uncorrelated fluctuations in the repetition frequencies of the two lasers due to perturbations, a patented synchronization system (SYNC) based on XPM [24] implements passive locking of the two oscillators [25,26], dynamically compensating for repetition frequency mismatches of up to 100 Hz. A 99/1 % beam splitter (TAP, Ruik, HPMFC-920-301F) and a photodetector (PD, Thorlabs, FDSP780) are used to monitor the laser repetition frequency. The splitter also acts as a polarizer, thus selecting a single polarization direction within the cavity. All components are connected using polarization-maintaining silica fibers: PM850 (Thorlabs) for the SESAM and PM780-HP (Thorlabs) for all other connections. These fibers are spliced with minimal losses due to good core matching.

3. Passively mode-locked laser modeling

To aid in the design and optimization of the SESAM-mode-locked Nd:fiber laser, we developed a custom MATLAB code specifically tailored for simulating mode-locked all-fiber lasers. The electric field of the pulse propagating in the cavity is described by its complex spectrum, whose phase describes spectral dispersion. By integrating the spectrum, one can determine the pulse energy and, by multiplying the latter by the repetition frequency, obtain the average power. A Fast Fourier Transform (FFT) is performed to retrieve the temporal profile of the pulse and its phase whenever considering effects better described in the time domain, such as the temporal phase term linked to self-phase modulation (SPM) and the nonlinear losses induced by a saturable absorber.

A small library of codes has been developed to describe the most common components of an all-fiber laser oscillator (passive and active single mode fiber, saturable absorber, FBG, splitter, coupler, circulator, WDM, filter, etc.). By running various combinations of these codes and selecting different parameters, it is possible to simulate and compare different cavity configurations. To describe propagation in fibers, the code utilizes the split-step Fourier method (SSFM), which facilitates the simultaneous implementation of both linear and nonlinear effects [27]. A passive fiber is described by its geometrical parameters, nonlinear index n_2 and wavelength-dependent second and third-order dispersion coefficients. Dealing with single-mode fibers, we assume a constant single-mode transverse profile. The mode field diameter (MFD) at

Optics EXPRESS

the operation wavelength is computed using Marcuse's equation [28] and used to determine the beam-core overlap and the effective nonlinear coefficient γ.

The dispersion and SPM are described at each split-step as phase terms in the spectral and temporal domains, respectively [29]. To simulate active fibers, in addition to implementing SPM and dispersion, we solve the rate equations with frequency-dependent cross-sections at each split-step to calculate the pump absorption and signal gain. For this process, we need to define additional parameters such as the upper-state lifetime, the doping concentration and the frequency-dependent effective cross-sections for absorption and emission. In linear oscillators, pulses pass through the active fiber twice per round-trip. As a result, the absorption of the pump and the amplification of the forward-propagating beam, i.e., the one co-propagating with the pump beam, are affected by the power of the backward-propagating beam, and vice versa. We implemented an iterative solution for the simultaneous propagation in the fiber of the pump beam and of both signal beams: starting with an informed initial estimate for the backward signal power at the fiber's start, we employ the modified Newton method to refine this guess until convergence is reached. The error estimate used by the algorithm is computed as the difference between the backward signal power at the fiber's end and the power obtained after propagating the forward beam at the end of the active fiber through the reflective system that follows the fiber.

Passively mode-locked lasers often present a SESAM, defined by its modulation depth, non-saturable losses, recovery time and saturation fluence. The saturation energy is calculated knowing the mode size on the absorber, which in our case corresponds to the mode field diameter of the fiber used in the connector. The saturation of the losses is influenced by the pulse duration: if the pulse duration exceeds the material's recovery time, a higher total pulse energy is needed to saturate the device. The developed model determines the effective energy experienced by the absorber at any moment by convolving the temporal profile of the pulse with the exponential response function of the absorber. As a result, time-dependent saturable absorber losses are computed. Reflection onto an FBG is described multiplying the pulse spectrum by the complex reflection coefficient, which determines the phase-induced chirp and the losses. The linear optical elements working in transmission, including WDMs and splitters, are accounted for by applying multiplicative factors to the field to represent the introduced losses, considering their spectral dependence when relevant. Finally, a constant loss is introduced for each splice between fibers.

To discuss the simulations performed on our specific setup, the oscillator can be described by three main elements: a SESAM, a Nd-doped active fiber and an FBG. The beam propagates between these three devices through passive fibers, which introduce dispersion and SPM, and other passive components, which introduce losses. Although these components are included in the simulations, for the sake of brevity they will not be mentioned in the following discussion. The most critical parameters employed in the simulations are reported in Table 1.

Figure 2(a) illustrates the iterative technique used to find a stable solution for the oscillator. An initial guess is taken by defining a few-picoseconds-long Gaussian pulse and its energy. The repetition frequency of the pulses, determined by the optical length of the cavity, links the pulse energy, needed to determine the nonlinear effects, with the average power, to be used in the rate equations. A round-trip in the cavity is simulated by describing the reflection on the FBG, followed by the iterative solution of the double pass in the active fiber, which includes the effect of the SESAM. After each round-trip, the last few values of the round-trip gain are analyzed: if the gain has been consistently close to one for a few round-trips, the simulation is interrupted and the pulse transmitted by the FBG is displayed. An additional exit condition based on the pulse energy is used to stop simulations when the pulse energy is vanishing, i.e., when the oscillator is operating below the lasing threshold.

Figure 2(b) shows how this technique is able to reach a self-consistent solution by simulating multiple round trips in the cavity starting from an initial guess. It should be noted that, although the algorithm's convergence dynamics share some similarities with the switch-on dynamics of a laser, they are not meant to describe them. The first panel shows the average power at the output

Optics EXPRESS

Table 1. Review of the main parameters employed in the simulations. The absorption and emission cross-sections of the active fiber are reported as a function of the wavelength in Fig. 3(a).

Component	Parameter	Value
Nd-doped active fiber	Length	1 m
	Core radius	2.5 µm
	Doping concentration	1.54×10^{25} m^{-3}
	Upper-state lifetime	0.45 ms
All fibers	Second-order dispersion	34×10^{-27} s^2/m
	Nonlinear index n_2	2.22×10^{-20} m^2/W
SESAM	Modulation depth	20 %
	Nonsaturable loss	10 %
	Relaxation time	3 ps
	Saturation fluence	15 µJ/cm^2
FBG	Output coupling transmission	11.7 %
	Dispersion	−2.97 ps^2
Intracavity components	Total saturated losses	6.5 dB

of the laser after different numbers of round trips. The second panel shows the active fiber gain for the forward and backward propagating beams (computed as the ratio between the pulse energy after propagation in the fiber and before) and the round trip gain (computed as the ratio between the pulse energy on the output coupler at one round trip and the one at the previous round trip), which remains unitary once the solution is found. The third panel shows the 3 dB pulse duration and spectral bandwidth at the laser output. Finally, the last panel shows the total pulse energy (dashed red line) on the saturable absorber and the maximum effective energy experienced by the absorber (solid red line), computed taking into account the temporal response of the device

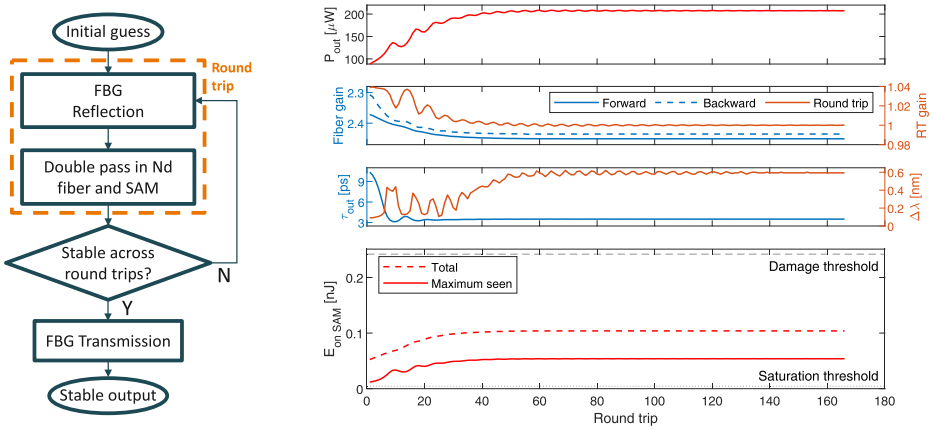

Fig. 2. (a) Simplified scheme of the convergence algorithm. (b) Example of the algorithm converging to a solution after multiple round trips, reporting (from top to bottom): the average output power; the active fiber gain (for the forward and backward propagating beams) and the round trip gain; the 3 dB pulse duration and spectral bandwidth; the total pulse energy on the saturable absorber and the maximum effective energy experienced by the absorber.

Optics EXPRESS

and the pulse duration. The model's ability to estimate the energy of the pulse reaching the saturable absorber was critical in designing the cavity, given the risk of damaging the SESAM when operating the laser at higher pump powers.

4. Results

Stable self-starting single-pulse mode-locking regime is obtained above a pump power threshold of ~70.5 mW. The laser emits pulse trains with 18.5 MHz repetition frequency at a central wavelength of 920.3 nm, as measured using an optical spectrum analyser (Anritsu, MS9740B).

As illustrated on the right axis in Fig. 3(a), Nd exhibits a primary emission peak near 1064 nm, where it operates as a four-level system. In our system, instead, operation is achieved on the weaker quasi-three-level transition at 920 nm, because of spectral filtering by the FBG in the cavity: the optical spectrum measured at the output of the laser, shown on the left axis (solid line) in Fig. 3(a), demonstrates a contrast of 22 dB between the two peaks. Integrating the optical spectrum, we estimated fluorescence to account for 20 to 25 % (depending on the pump power) of the power at the output of the laser.

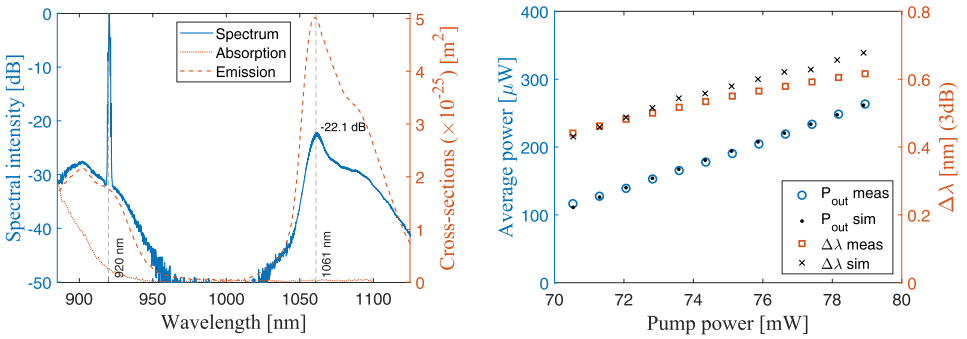

Fig. 3. (a) Measured spectral intensity with respect to the peak (solid line, left axis) for 79 mW pump power and absorption (dotted line) and emission (dashed line) cross-sections of the Nd-doped active fiber (right axis). (b) Measured (blue circles) and simulated (black dots) average power at the output of the laser (left axis) and measured (orange squares) and simulated (black cross marks) 3 dB spectral bandwidth (right axis) in mode-locking operation, as a function of the pump power on the active fiber.

Figure 3(b) shows on the left axis the input-output power characteristic of the mode-locked Nd-doped fiber laser (blue circles), obtained measuring with a powermeter (Thorlabs, PM16-130) and subtracting the fluorescence estimated from the optical spectrum. A laser slope efficiency of 1.7 % (with respect to the pump power on the active fiber) was experimentally observed and the maximum average output power in single pulse operation was 263 µW at ~79 mW pump power. We limited the pump power at this level to keep the intensity of the Kelly sidebands at −3 dB with respect to the main peak of the laser spectrum and to reduce the risk of SESAM damaging. The right axis of Fig. 3(b) reports the 3 dB optical spectral bandwidth (orange squares), showing an increase with the pump power from 0.44 nm to 0.62 nm in mode-locking regime. The simulation results corresponding to these measurements are reported with black dots for the average power and black cross marks for the 3 dB optical spectral bandwidth. Both show good agreement with the experimental results, confirming the validity of the model.

Figure 4(a) shows the measured optical spectrum together with the computed spectrum and spectral phase for a pump power of 79 mW. The simulations align well with the experimental data, reproducing the measured spectrum with its Kelly sidebands. Figure 4(b) shows the simulated

Optics EXPRESS

pulse profile and temporal phase for a pump power of 79 mW. Due to the limited power of the pulse train, direct measurement of the pulse duration is not feasible without a low-dispersion optical amplifier. Nonetheless, given the overall good agreement between the simulated results and the available measurements, and given the deterministic Fourier transform relationship between the spectral and temporal domain, we also expect the experimental pulse shape to closely resemble the simulated one.

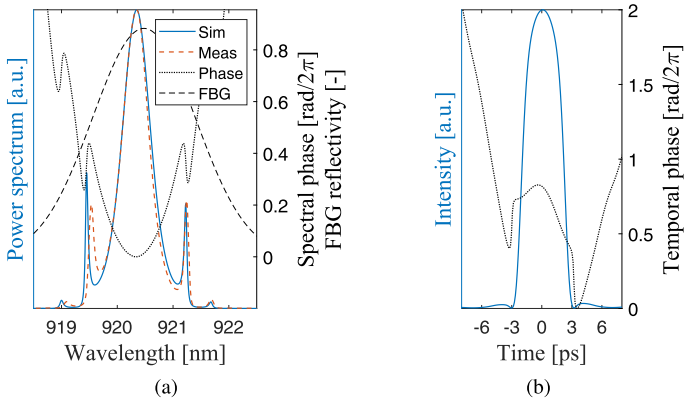

Fig. 4. (a) Simulated (solid line) and measured (dashed line) normalized optical spectra (left axis) and simulated spectral phase (dotted line, right axis) for 79 mW pump power; FBG reflectivity (dashed line, right axis) as tested by the supplier. (b) Simulated optical pulse (solid line, left axis) and its temporal phase (dotted line, right axis) for 79 mW pump power.

To characterize the stability of both the intensity and repetition frequency of the pulse train generated by the Nd-fiber mode-locked laser, a thorough investigation of the current generated at the output of a fast photodetector (ThorLabs, PDA05CF2) was conducted. Figure 5(a) shows the temporal trace of the pulse trains recorded on an oscilloscope (LeCroy, WaveSurfer 3104z) and Figure 5(b) reports the corresponding radiofrequency (RF) spectrum measured by an RF spectrum analyzer (Agilent, E4445A). The RF spectrum reveals a pure mode-locking regime without any Q-switching instability. No sidebands are observed around the pulse repetition frequency peak, which is characterized by a signal to noise ratio (SNR) larger than 100 dB in a resolution bandwidth of 1 kHz.

To further characterize the stability of the laser intensity and pulse repetition frequency, the same photodetector and RF spectrum analyzer were used to measure the power spectral density of the relative intensity noise (RIN) and the phase noise of the repetition frequency. Figure 6(a) reports the power spectral density of the RIN of the laser against the background noise of the photodetector in the Fourier frequency range from 10 Hz to 9.25 MHz (half of the repetition frequency). For Fourier frequency lower than 10 kHz, the RIN is characterized by flicker and $1/f^2$ noise power spectral densities due to the typical intensity noise contribution of the pump diode, reaching a RIN level of −120 dB at 10 kHz. For higher frequencies values, the RIN is nearly constant up to 100 kHz and for higher frequencies it is further reduced by the filtering effect of the finite lifetime of the laser level of the Nd ion, reaching for frequencies higher than 5 MHz a noise level of −143 dB/Hz, 11 dB higher than the shot noise level. Within the broad integration bandwidth from 50 Hz to 9.25 MHz, the mode-locked Nd-fiber laser shows a RIN of just 0.04 %.

Using the same electrical spectrum analyzer, the phase noise power spectral density of the pulse repetition frequency is also measured. Figure 6(b) reports the recorded phase noise power spectral densities of the fundamental and fourth harmonic of the pulse repetition frequency. For Fourier frequencies above 600 Hz, the phase noise spectral densities of the fourth harmonic and

Optics EXPRESS

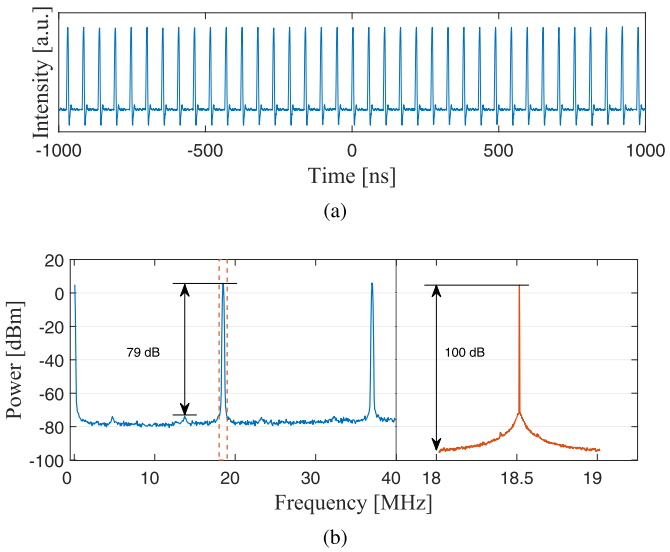

Fig. 5. (a) Temporal trace of the photodetector signal for 79 mW pump power. (b) RF spectrum of the same photodetector signal. On the left, the spectrum is shown up to the second harmonic of the repetition frequency of the pulses, with a 100 kHz resolution bandwidth. On the right, the fundamental peak at the repetition frequency is shown with a 1 kHz resolution bandwidth.

the fundamental have equal values, which is a clear indication that for this Fourier frequency range the phase noise measurements are dominated by the RIN of the Nd-fiber laser. For frequencies lower than 600 Hz the phase noise of the fourth harmonic component can be clearly discriminated with respect to the laser RIN contribution. From the power spectral density of the phase noise of the fourth harmonic component, a root-mean-square phase noise of 0.9 mrad is computed in the integration bandwidth from 50 Hz to 9.25 MHz. It is worth noting that this level is an upper limit, being the recorded phase noise mainly limited by the laser RIN for Fourier frequency higher than 600 Hz. This phase noise translates in an upper level timing jitter of the fundamental

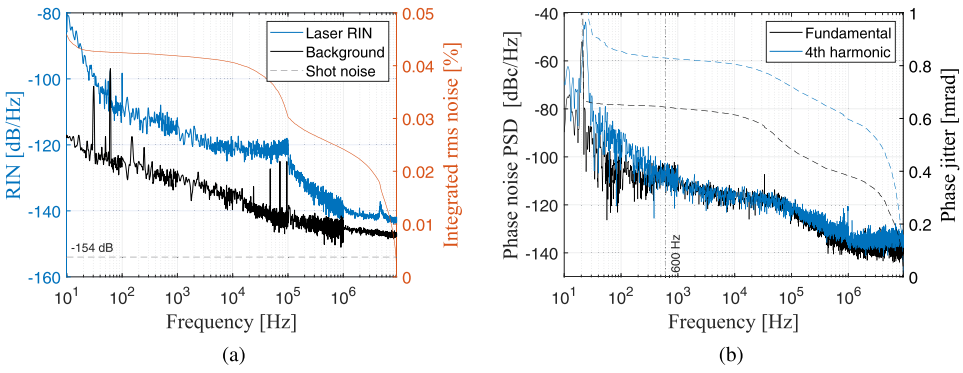

Fig. 6. (a) RIN (left axis) and integrated rms noise (right axis) of the laser for 79 mW pump power, as a function of the frequency. (b) Power spectral density of the phase noise (solid line, left axis) and phase jitter (dashed line, right axis) of the fundamental peak (black) and its fourth harmonic (blue) for 79 mW pump power, as a function of the frequency.

Optics EXPRESS

pulse repetition frequency of 0.9 mrad/$(2\pi \cdot 4 f_{\mathrm{rep}}) = 1.9$ ps in the whole bandwidth from 50 Hz to 9.25 MHz.

Finally, using a photodetector (Thorlabs, DET08CFC) connected to an electronic frequency counter (Liquid Instruments, Moku:Lab), also the time domain stability of the pulse repetition frequency is measured. Figure 7 shows the Allan deviation [30] of the repetition frequency of the laser as a function of the averaging time, τ, in the medium term range from 0.2 ms to 20 s. The Allan deviation, $\sigma(\tau)$ in Hz unit, is well fitted by the curve $\sigma(\tau) = \left(h_2\tau^{-2} + h_{-2}\tau\right)^{1/2}$, the quadrature sum of a white phase noise contribution with a polynomial coefficient $h_2 = 2.4 \times 10^{-9}$ and a random walk frequency noise with a coefficient $h_{-2} = 2.3$ Hz^3 [30]. A minimum Allan deviation of 70 mHz (corresponding to a fractional deviation of 3.8×10^{-9}) is observed at 1-ms averaging time.

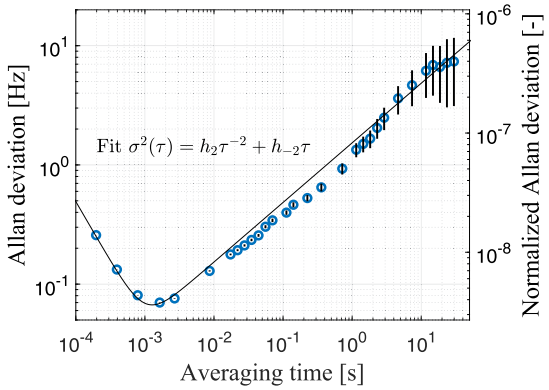

Fig. 7. Allan deviation of the repetition frequency of the laser (circles) for different averaging times and fitting curve (solid lines) $\sigma^2(\tau) = h_2\tau^{-2} + h_{-2}\tau$, with $h_2 = 2.4 \times 10^{-9}$ and $h_{-2} = 2.3$ Hz^3. Error bars represent the 1-sigma confidence interval.

The previous measurements were performed while the XPM-based synchronization system was inactive. This system, whose technical details fall beyond the scope of this article, enables passive locking of the repetition frequencies of two lasers by inducing optical cavity length adjustments in both oscillators, compensating in real time for minor frequency mismatches. To showcase the ability to lock the laser's repetition frequency to two additional oscillators, the laser was synchronized with an Er-doped fiber ring oscillator, which was itself locked to a broadband Yb-doped fiber linear oscillator using the same approach [31], as schematically illustrated in Fig. 8(a). Figure 8(b) depicts the drift over time of the pulse repetition frequencies of the Nd- and Yb-doped oscillators, referenced to the Nd frequency at time $t = 0$. For negative timestamps, the drift is presented over a narrow range of just 1 Hz to highlight the exceptional overlap between the two repetition frequencies, demonstrating that all three oscillators are synchronized. For positive timestamps, a broader frequency range is used to reveal the dynamics that follow a strong mechanical perturbation of the resonators at $t = 15$ s, which temporarily disrupts their repetition frequencies. Initially, the synchronization mechanism cannot correct the near-100 Hz mismatch in repetition frequencies between the lasers; however, synchronization is reestablished a few seconds after the perturbation has passed, when the unlocked frequency mismatch reduces to 84 Hz. In an unperturbed laboratory environment, without any active temperature control, pulse synchronization is maintained for several hours.

Lastly, an average power of 250 mW was reached using a yet unpublished FBG-enabled two-stage Nd-doped fiber amplifier, which incorporates an acousto-optic modulator and a tunable delay line necessary for SRS microscopy. Additionally, simulations have shown that by optimizing the FBG dispersion and fiber lengths of this amplifier it is possible to reach the same output power level with a 3 dB optical bandwidth of 1 nm and a pulse duration of 2 ps.

Optics EXPRESS

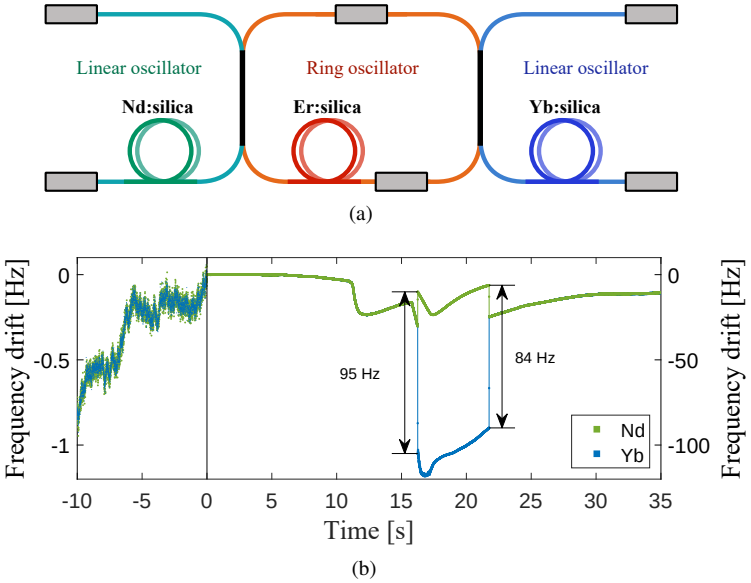

Fig. 8. (a) Simplified scheme of the three synchronized oscillators, with shared passive synchronization fibers represented in black. (b) Drift in time of the repetition frequencies of the Nd and Yb-doped oscillators, with respect to frequency of Nd at $t = 0$. For $t<0$ the drift is shown in a 1 Hz range (left axis), while for $t>0$ the range is 100 Hz (right axis).

5. Conclusion

In conclusion, we have successfully developed and characterized a passively mode-locked Nd-doped all-polarization-maintaining-fiber laser emitting at 920 nm, to be used as the pump laser in an SRS microscope. The system, optimized using a combination of simulations and experiments, demonstrates reliable generation of stable self-starting trains of ultrashort pulses with a repetition frequency of 18.5 MHz and an average output power of 0.26 mW. The compact and robust laser is characterized by high stability levels of pulse intensity and repetition frequency, as experimentally demonstrated by an integrated RIN of 0.04% and a pulse timing jitter below 2 ps, respectively, in an integration bandwidth from 50 Hz to 9.25 MHz. After dispersion-managed amplification, the output power can reach 250 mW with a 3 dB spectral bandwidth of 1 nm and a pulse duration of 2 ps, thus meeting the requirements for spectral and temporal resolution in biomedical nonlinear imaging techniques such as coherent Raman imaging. Specifically, having demonstrated the ability to lock the repetition frequency to the one of an Yb-doped oscillator, this laser will enable broadband SRS microscopy in the fingerprint region.

Funding. Ministero dell'Università e della Ricerca (IR0000016, ID D2B8D520, CUP B53C22001750006); European Union's Horizon Europe research and innovation programme (101058004 – CHARM).

Acknowledgment. G. Cerullo and G. Galzerano acknowledge financial support by the European Union's NextGenerationEU Programme with the I-PHOQS Infrastructure [IR0000016, ID D2B8D520, CUP B53C22001750006] Integrated infrastructure initiative in PHOtonic and Quantum Sciences. Matteo Negro and Giulio Cerullo acknowledge support from European Union's Horizon Europe research and innovation programme under grant agreement No 101058004 – CHARM.

Disclosures. Gabriele Di Noia, Francesco Crisafi, Matteo Negro and Giulio Cerullo disclose association with Cambridge Raman Imaging S.r.l., which aims to commercialize broadband SRS microscopes.

Data availability. According to the open data policies of the Physics Department of Politecnico di Milano, all data underlying the results presented in this paper are publicly available in [32].

Optics EXPRESS

References

1. C. Krafft, I. W. Schie, T. Meyer, *et al.*, "Developments in spontaneous and coherent Raman scattering microscopic imaging for biomedical applications," Chem. Soc. Rev. **45**(7), 1819–1849 (2016).
2. C. W. Freudiger, W. Min, B. G. Saar, *et al.*, "Label-Free Biomedical Imaging with High Sensitivity by Stimulated Raman Scattering Microscopy," Science **322**(5909), 1857–1861 (2008).
3. B. G. Saar, C. W. Freudiger, J. Reichman, *et al.*, "Video-rate molecular imaging in vivo with stimulated raman scattering," Science **330**(6009), 1368–1370 (2010).
4. J.-X. Cheng and X. S. Xie, "Vibrational spectroscopic imaging of living systems: An emerging platform for biology and medicine," Science **350**(6264), aaa8870 (2015).
5. A. De la Cadena, F. Vernuccio, A. Ragni, *et al.*, "Broadband stimulated Raman imaging based on multi-channel lock-in detection for spectral histopathology," APL Photonics **7**(7), 076104 (2022).
6. D. Polli, V. Kumar, C. M. Valensise, *et al.*, "Broadband coherent raman scattering microscopy," Laser Photonics Rev. **12**(9), 1800020 (2018).
7. M. Brinkmann, A. Fast, T. Hellwig, *et al.*, "Portable all-fiber dual-output widely tunable light source for coherent raman imaging," Biomed. Opt. Express **10**(9), 4437 (2019).
8. K. Kieu, *Compact fiber lasers for stimulated Raman scattering microscopy* (Elsevier, 2022), pp. 233–255.
9. A. Gambetta, V. Kumar, G. Grancini, *et al.*, "Fiber-format stimulated-raman-scattering microscopy from a single laser oscillator," Opt. Lett. **35**(2), 226–228 (2010).
10. C. W. Freudiger, W. Yang, G. R. Holtom, *et al.*, "Stimulated raman scattering microscopy with a robust fibre laser source," Nat. Photonics **8**(2), 153–159 (2014).
11. K. Yang, Y. Shen, J. Ao, *et al.*, "Passively synchronized mode-locked fiber lasers for coherent anti-Stokes Raman imaging," Opt. Express **28**(9), 13721–13730 (2020).
12. K. Nose, T. Kishi, Y. Ozeki, *et al.*, "Stimulated Raman spectral microscope using synchronized Er- and Yb-fiber lasers," Jpn. J. Appl. Phys. **53**(5), 052401 (2014).
13. F. Crisafi, B. Talone, A. Ragni, *et al.*, "Plug-And-Play Stimulated Raman Microscopy System for Broadband Coherent Vibrational Imaging," in *Conference on Lasers and Electro-Optics Europe & European Quantum Electronics Conference* (2023), p. 1–1.
14. F. Crisafi, B. Talone, A. Ragni, *et al.*, "A compact, turn-key platform for multiplex stimulated raman scattering microscopy," in *Biomedical Vibrational Spectroscopy 2024: Advances in Research and Industry*, Z. Huang, ed. (SPIE, 2024), p. 28.
15. M. Li, W. Yang, Z. Zhang, *et al.*, "Mode-locked femtosecond 910 nm nd:fibre laser with phase biased non-linear loop mirror," Electron. Lett. **53**(22), 1479–1481 (2017).
16. R. Becheker, M. Tang, M. Touil, *et al.*, "Dissipative soliton resonance in a mode-locked Nd-fiber laser operating at 927 nm," Opt. Lett. **44**(22), 5497 (2019).
17. A. A. Mkrtchyan, Y. G. Gladush, M. A. Melkumov, *et al.*, "Nd-doped polarization maintaining all-fiber laser with dissipative soliton resonance mode-locking at 905 nm," J. Lightwave Technol. **39**(17), 5582–5588 (2021).
18. S. Wang, Y. Li, Y. Chen, *et al.*, "Femtosecond all-polarization-maintaining Nd fiber laser at 920 nm mode locked by a biased NALM," Opt. Express **29**(23), 38199 (2021).
19. R. Hofer, M. Hofer, G. A. Reider, *et al.*, "Modelocking of a Nd-fiber laser at 920 nm," Opt. Commun. **140**(4-6), 242–244 (1997).
20. X. Gao, W. Zong, B. Chen, *et al.*, "Core-pumped femtosecond Nd:fiber laser at 910 and 935 nm," Opt. Lett. **39**(15), 4404 (2014).
21. K. Qian, H. Wang, M. Laroche, *et al.*, "Mode-locked nd-doped fiber laser at 930 nm," Opt. Lett. **39**(2), 267 (2014).
22. K. Le Corre, T. Robin, B. Cadier, *et al.*, "Mode-locked all-PM nd-doped fiber laser near 910 nm," Opt. Lett. **46**(15), 3564 (2021).
23. A. A. Mkrtchyan, M. S. Mishevsky, Y. G. Gladush, *et al.*, "Dispersion Managed Mode-locking in all-fiber Polarization-maintaining Nd-doped Laser at 920 nm," J. Lightwave Technol. **41**(8), 2494–2500 (2023).
24. G. P. Agrawal, "Induced-frequency shift of copropagating ultrafast optical pulses," (1939).
25. F. Crisafi, G. Di Noia, and M. Negro, "An optical circuit arrangement (patent GB2621150A)," (2023).
26. W. Li, Q. Hao, Y. Li, *et al.*, "Ultrafast Laser Pulse Synchronization," in *Coherence and Ultrashort Pulse Laser Emission* (IntechOpen, 2010).
27. M. Hamza and S. Tariq, "Split Step Fourier Method Based Pulse Propagation Model for Nonlinear Fiber Optics," in *International Conference on Electrical Engineering* (2007), pp. 1–5.
28. D. Marcuse, "Loss analysis of single-mode fiber splices," Bell Syst. Tech. J. **56**(5), 703–718 (1977).
29. G. P. Agrawal, *Nonlinear Fiber Optics* (Academic Press, 2013).
30. D. Allan, "Statistics of atomic frequency standards," Proc. IEEE **54**(2), 221–230 (1966).
31. F. Crisafi, G. Di Noia, F. Pisani, *et al.*, "A fiber laser source for parallel dual-window multiplex SRS (DWM-SRS): single-shot CH-stretching and fingerprint imaging," in *Label-free Biomedical Imaging and Sensing*, vol. 13331 N. T. Shaked and O. Hayden, eds. (SPIE, 2025), pp. 132–139.
32. F. Pisani and G. Galzerano, "Data regarding the article "SESAM mode-locked Nd:fiber laser at 920 nm for nonlinear optical microscopy"," Zenodo (2025), https://doi.org/10.5281/zenodo.13908731.